HMG Advance Access published June 20, 2012

*Human Molecular Genetics, 2012* **1–14**
*doi:10.1093/hmg/dds217*

# Retrocochlear function of the peripheral deafness gene Cacna1d

**Somisetty V. Satheesh[1,†], Katrin Kunert[3,†], Lukas Rüttiger[4], Annalisa Zuccotti[4], Kai Schönig[3], Eckhard Friauf[5], Marlies Knipper[4], Dusan Bartsch[3,‡] and Hans Gerd Nothwang[1,2,*,‡]**

[1]Department of Neurogenetics and [2]Center for Neuroscience, Carl von Ossietzky University Oldenburg, 26111 Oldenburg, Germany, [3]Department of Molecular Biology, Central Institute of Mental Health and Medical Faculty Mannheim, Heidelberg University, 68159 Mannheim, Germany, [4]Department of Otolaryngology, Hearing Research Centre Tübingen (THRC), Molecular Physiology of Hearing, University of Tübingen, Elfriede Aulhorn Str. 5, 72076 Tübingen, Germany and [5]Department of Biology, Animal Physiology Group, University of Kaiserslautern, POB 3049, D-67663 Kaiserslautern, Germany

Received April 12, 2012; Revised and Accepted May 30, 2012

**Hearing impairment represents the most common sensory deficit in humans. Genetic mutations contribute significantly to this disorder. Mostly, only malfunction of the ear is considered. Here, we assessed the role of the peripheral deafness gene *Cacna1d*, encoding the L-type channel $Ca_v1.3$, in downstream processing of acoustic information. To this end, we generated a mouse conditional *Cacna1d-eGFP$^{flex}$* allele. Upon pairing with *Egr2::Cre* mice, $Ca_v1.3$ was ablated in the auditory brainstem, leaving the inner ear intact. Structural assessment of the superior olivary complex (SOC), an essential auditory brainstem center, revealed a dramatic volume reduction (43–47%) of major nuclei in young adult *Egr2::Cre;Cacna1d-eGFP$^{flex}$* mice. This volume decline was mainly caused by a reduced cell number (decline by 46–56%). Abnormal formation of the lateral superior olive was already present at P4, demonstrating an essential perinatal role of $Ca_v1.3$ in the SOC. Measurements of auditory brainstem responses demonstrated a decreased amplitude in the auditory nerve between 50 and 75 dB stimulation in *Egr2::Cre;Cacna1d-eGFP$^{flex}$* knockout mice and increased amplitudes in central auditory processing centers. Immunohistochemical studies linked the amplitude changes in the central auditory system to reduced expression of $K_v1.2$. No changes were observed for $K_v1.1$, KCC2, a determinant of inhibitory neurotransmission, and choline acetyltransferase, a marker of efferent olivocochlear neurons. Together, these analyses identify a crucial retrocochlear role of $Ca_v1.3$ and demonstrate that mutations in deafness genes can affect sensory cells and neurons alike. As a corollary, hearing aids have to address central auditory processing deficits as well.**

## INTRODUCTION

Hearing disorders are the most common sensory deficit in humans and represent a heavy social and economic burden to individuals and societies alike (1). About 1–2 newborns in 1000 and more than half of the elderly experience hearing loss (2). It is estimated that half of all childhood deafness is due to hereditary causes (2,3). Genetic analyses have identified mutations in more than 50 genes, which have been linked to hearing impairment. Most mutations were shown to disrupt cochlear function (2,4,5). However, the precise pathogenic mechanisms are far from being fully understood (2,6).

In many cases of hearing impairment, hearing devices such as cochlear implants are prescribed to achieve well-functioning hearing. However, the benefit from these devices is often low (5,7). One reason for the poor outcome might be that perception of acoustic information requires accurate assembly and proper function throughout the auditory system. Yet, in the central

*To whom correspondence should be addressed at: Department of Neurogenetics, Carl von Ossietzky University Oldenburg, 26111 Oldenburg, Germany. Tel: +49 4417983932; Fax: +49 4417985649; Email: hans.g.nothwang@uni-oldenburg.de
†The authors contributed equally to the manuscript.
‡Shared senior authorship.

auditory system, the function of genes associated with hearing impairment has rarely been addressed (8,9).

One of the essential genes in inner ear cells is *Cacna1d*, which encodes the pore-forming α1D subunit ($Ca_v1.3$) of L-type voltage-dependent calcium channels (LTCCs) (10). Cav1.3 channels are essential for neurotransmitter release from inner hair cells onto auditory nerve fibers (11). In humans, cosegregation of a mutation in *Cacna1d* with deafness was reported in two families (12). In efforts to dissect the role of cochlea-driven activity for the development of central auditory structures, *Cacna1d*$^{-/-}$ mice with ubiquitous ablation of $Ca_v1.3$ were recently analyzed in the auditory brainstem as well. In the superior olivary complex (SOC), an important auditory structure involved in sound localization (13,14), larger NMDA-receptor mediated excitatory postsynaptic currents were reported in P14–17-old *Cacna1d*$^{-/-}$ mice (15). A further study demonstrated reduced volumes of its major nuclei, changes in biophysical properties and altered gene expression (16). However, both studies did not address whether these anomalies were due to the lack of peripheral activity, as initially proposed (15). Based on the functional expression of $Ca_v1.3$ in the SOC (16,17) as well as the abnormal auditory brainstem structures in *Cacna1d*$^{-/-}$ mice not observed in other deaf mice models, an important on-site role of $Ca_v1.3$ in the SOC was suggested as an alternative (16). Since essential retrocochlear functions of peripheral deafness genes will cause a pleiotropic phenotype in the auditory system, thereby affecting auditory rehabilitation, we set out to test the hypothesis of an important function of $Ca_v1.3$ in the central auditory system. We therefore generated a mouse with a targeted ablation of the gene in the central auditory brainstem to circumvent peripheral deafness. This approach revealed an important retrocochlear role of $Ca_v1.3$. Furthermore, it established *Cacna1d-eGFP*$^{flex}$ mice as a valuable mouse model not only to investigate central auditory processing disorders (CAPD) but also to study other physiological functions of the $Ca_v1.3$ calcium channel.

## RESULTS

### Generation and analyses of Cacna1d-eGFP$^{flex}$, EIIa::Cre;Cacna1d-eGFP$^{flex}$ and Egr2::Cre;Cacna1d-eGFP$^{flex}$ mouse lines

To study the potential on-site role of $Ca_v1.3$ in the SOC, we generated mice with a conditional *Cacna1d* allele for spatially restricted gene ablation. To easily monitor recombination events on the single cell level, we used the Cre/loxP-based FLEX system [Flip excision (18)], in which the ablation of *Cacna1d* is coupled to the expression of the reporter gene *eGFP* under the control of the *Cacna1d* promoter (Fig. 1A). To test for functionality, the targeting construct was tansfected in HeLa cells under control of the constitutively active Caggs promoter. Cotransfection with Cre-recombinase resulted in expression of eGFP, whereas no signal was obtained in the absence of Cre-recombinase (Fig. 1B and C).

Next, we wanted to analyze whether the transgene allele faithfully recapitulates the expression of the endogenous *Cacna1d* allele. We therefore crossed *Cacna1d-eGFP*$^{flex}$ with *EIIa::Cre* deleter mice. The adenovirus *EIIa* promoter is already active in the ovum at the time of fertilization which leads to *Cre*-recombination when the embryo is still at the one-cell zygote stage (19,20). Thus, all cells of the developing animal will have the inverted DNA sequence and the eGFP expression driven by the *Cacna1d* regulatory elements is germline transmissible in the absence of Cre expression. Diaminobenzidine (DAB) immunohistochemistry with antibodies against eGFP revealed a strong staining in several brain regions, demonstrating *in vivo* functional expression of eGFP. In a sagittal section through the entire brain, moderate to strong staining was observed in the cerebral cortex, the olfactory bulb, the superior colliculus and the adjacent optic tract, and the cerebellum (Fig. 2A). Further analyses revealed moderate staining in the periventricular nucleus in the thalamus (Fig. 2B), as well as in various brainstem areas, such as the locus coeruleus, the facial nucleus and the cuneate nucleus (Fig. 2C). Additionally, staining was observed in the hippocampus, in the subventricular zone and in the amygdala (data not shown). Transgenic littermates with no expression of Cre-recombinase showed no staining for eGFP (Fig. 2D). Altogether, the expression pattern of eGFP closely matched the previously reported presence of *Cacna1d* in the cerebral cortex (21), the cerebellum (22), the olfactory bulb (23–25), the paraventricular nucleus (26) and brainstem structures (27). Given the lack of reliable antibodies against $Ca_v1.3$, the *Cacna1d-eGFP*$^{flex}$ mouse will hence be an important reporter line to analyze $Ca_v1.3$ expression.

To investigate the on-site role of $Ca_v1.3$ in the auditory brainstem, we paired *Cacna1d-eGFP*$^{flex}$ animals with *Egr2::Cre* mice. This Cre driver mouse line mediates recombination in rhombomeres 3 and 5 of the embryonic neural tube, allowing genetic manipulation of neuronal populations in the auditory brainstem such as the lateral superior olive (LSO) and medial nucleus of the trapezoid body (MNTB) (Fig. 3C and D) (28–31). Importantly, the cochlea is spared from Cre-mediated recombination (Fig. 3A and B). To analyze the extent of Cre expression in the auditory brainstem in this Cre driver line, we also analyzed the inferior colliculus, the principal midbrain structure of the auditory pathway. Like in the cochlea, no X-gal staining was observed (Fig. 3E and F). Hence, recombination in *Egr2::Cre* mice is confined to auditory structures in the hindbrain.

Deletion of $Ca_v1.3$ in *Egr2::Cre;Cacna1d-eGFP*$^{flex}$ animals (*Cacna1d*$^{cko}$ in the following) was detected via immunohistochemistry against eGFP. To avoid overlapping signals from eGFP, an Alexa-Fluor 594-labeled secondary antibody was used, which gives rise to red fluorescence. Indeed, eGFP was detected in the LSO and MNTB of *Cacna1d*$^{cko}$ both at P4 and P25 (Fig. 4B, D, F, H). In contrast, no specific labeling was observed in auditory structures where Cre-recombinase is not expressed such as the inferior colliculus (Fig. 4J and L) and in littermates lacking Cre-recombinase (Fig. 4A, C, E, G, I, K). Since eGFP faithfully mirrors expression of *Cacna1d* (Fig. 2), these data demonstrate expression of *Cacna1d* throughout the SOC during postnatal development. Indeed, RT–PCR analyses using two different primer pairs confirmed expression of *Cacna1d* in wild-type SOC tissue both at P4 and P25 (Fig. 4M). These data are in excellent agreement with electrophysiological analysis of P4 and P12 LSO neurons (17) and $Ca^{2+}$ imaging using *Fura-2* in P3 LSO neurons (16), which

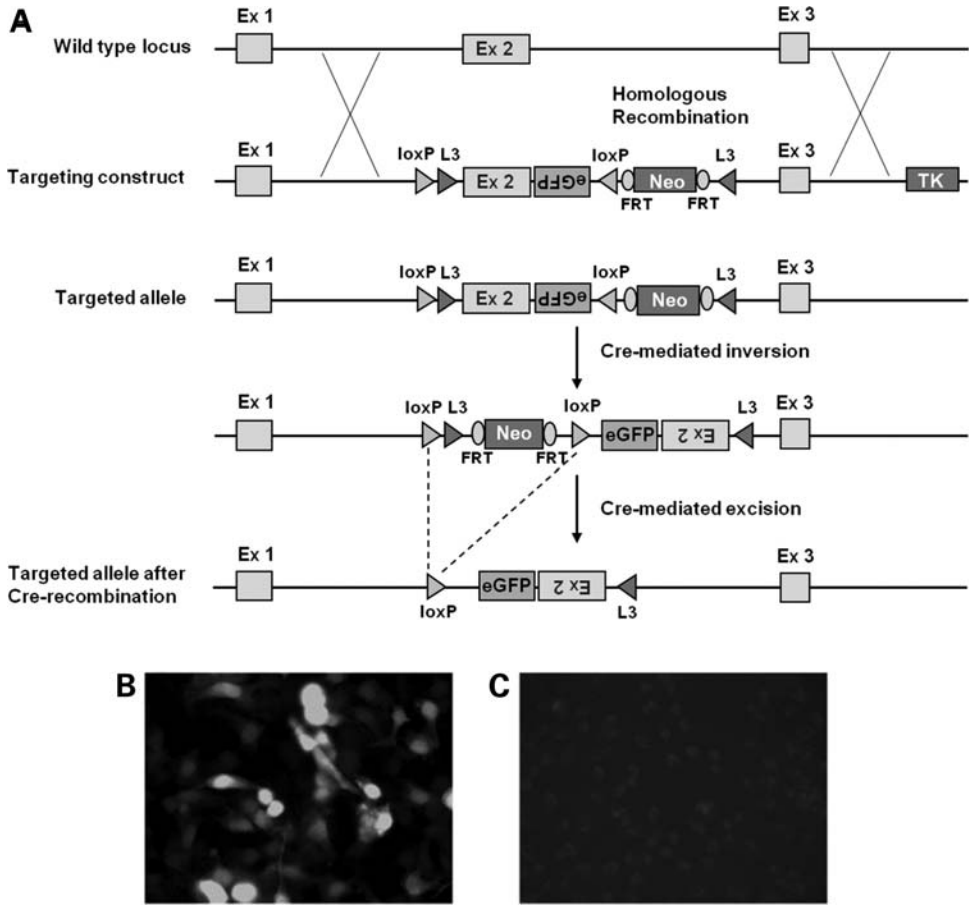


**Figure 1.** Generation of a mouse conditional *Cacna1d-eGFP*$^{flex}$ allele. (**A**) Schematic drawing of the targeting strategy. The Flex allele consists of two pairs of heterotypic *LoxP* (light gray) and mutant *L3* (dark gray) sites, which are alternately arranged in head-to-head orientation. Between the two pairs, an eGFP-encoding open reading frame followed by a polyadenlyation signal (pA) and a splice acceptor site (SA) was inserted in antisense orientation downstream to exon 2. Upon Cre-mediated recombination, the exon 2-eGFP cassette is irreversibly inverted, resulting in eGFP expression under control of the *Cacna1d* regulatory region and simultaneously preventing endogenous *Cacna1d* expression (eGFP knock-in in *Cacna1d*). The *neo* cassette required for positive selection in embryonic stem cells is flanked by FRT sites for deletion by Flpe recombinase. (**B** and **C**) *In vitro* functionality of the targeting construct. A modified targeting construct under the control of the Caggs promoter was transfected in HeLa cells together with a Cre expressing plasmid (B) or control DNA (C). Images show representative results of three independent experiments.

both demonstrated functional $Ca_v1.3$ in the SOC. They also confirm a previous immunohistochemical study, which identified $Ca_v1.3$ in the adult mouse SOC (32).

## Immunohistochemical analyses of the SOC in *Cacna1d*$^{cko}$ animals

To examine the integrity of the SOC, we performed immunohistochemistry for Vglut1, a marker for excitatory inputs onto SOC neurons (33) using P4 and P25 coronal brainstem sections (Fig. 5A–D). Interestingly, the LSO of young-adult *Cacna1d*$^{cko}$ mice lacked the U shape present in wild-type animals (Fig. 5A and B). Instead, a more round shape was found. Analyses of Nissl-stained sections revealed that its volume was reduced by 43% (wild-type: $0.0253 \pm 0.0029\ mm^3$; *Cacna1d*$^{cko}$: $0.0143 \pm 0.0031\ mm^3$, $P < 0.001$) (Fig. 5E). Likewise, the MNTB volume was reduced by 47% (wild-type: $0.0439 \pm 0.0045\ mm^3$; *Cacna1d*$^{cko}$: $0.0231 \pm 0.0029\ mm^3$, $P < 0.001$) (Fig. 5G). In contrast, there was no significant difference in the volume of the LSO or MNTB between *Cacna1d*$^{fl/fl}$ (control) and heterozygous knockout animals (Fig. 5E and G). Cell counts in Nissl-stained sections revealed that the smaller volumes in both nuclei were due to a reduced number of neurons [LSO, wild-type: $1511 \pm 153$, *Cacna1d*$^{cko}$: $694 \pm 27$ (46%), $P < 0.001$; MNTB, wild-type: $4095 \pm 594$, *Cacna1d*$^{cko}$: $2310 \pm 260$ (56%), $P < 0.001$] (Fig. 5F and H). These changes on the anatomical and cellular level were similar to those observed in *Cacna1d*$^{-/-}$ animals (16).

Vglut1 immunohistochemistry in P4 animals demonstrated a malformed LSO already at this neonatal stage (Fig. 5C and D). Altogether, these data indicate an essential on-site role of $Ca_v1.3$ for proper development of the SOC.

## Auditory brainstem responses in *Cacna1d*$^{cko}$ animals

We next assessed the functional consequences of loss of $Ca_v1.3$ for auditory physiology by analyzing auditory brainstem responses (ABR) and distortion product otoacoustic emission (DPOAE). ABR thresholds for pure tone, click and noise burst stimuli were similar for control and *Cacna1d*$^{cko}$

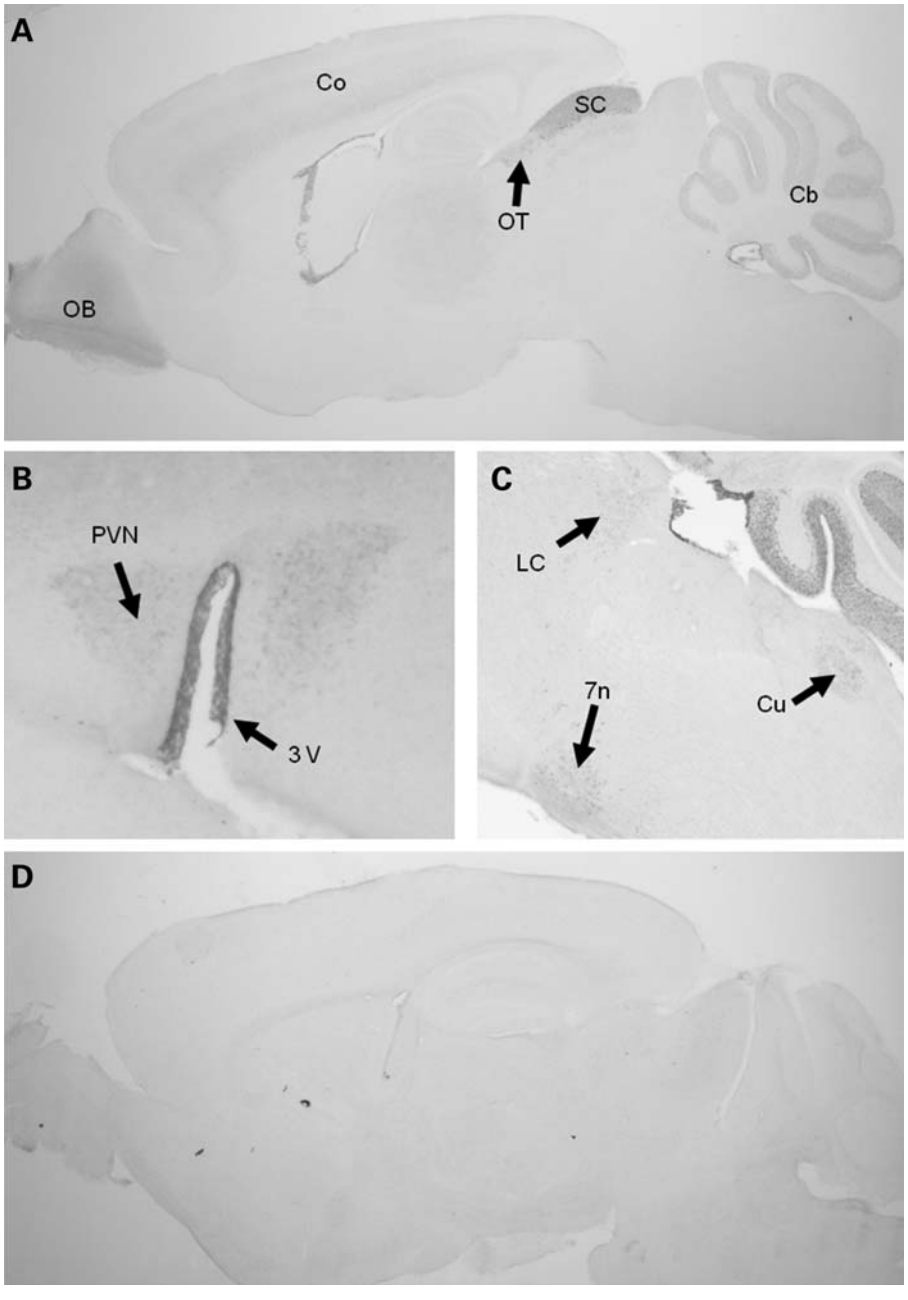


**Figure 2.** Expression of eGFP in the brain of *EIIa::Cre*;*Cacna1d-eGFP*$^{flex}$ mice. DAB-immunohistochemistry using antibodies against the reporter protein eGFP. (**A**) Overview of a sagittal brain section with staining in the olfactory bulb, the cerebral cortex, the optic tract, the superior colliculus and the cerebellum. (**B**) Coronal section at the level of the thamalus, revealing staining of the paraventricular nucleus. (**C**) Sagittal brainstem section with staining in the locus coeruleus, the facial nucleus and the cuneate nucleus. (**D**) Sagittal brain section of a single transgenic *Cacna1d-GFP*$^{flex}$ littermate, showing no staining. At least two brains were analyzed per area. 3 V, third ventricle; 7n, facial nucleus; Cb, cerebellum; Co, cortex; Cu, cuneate nucleus; LC, locus coeruleus; OB, olfactory bulb; OT, optic tract; PVN, paraventricular nucleus; SC, superior colliculus.

animals (Fig. 6A), demonstrating normal function of inner hair cells in *Cacna1d*$^{cko}$ mice, which is in contrast to the ubiquitous *Cacna1d* knockout mice (11). DPOAE thresholds were only slightly ($<$10 dB), but significantly increased in the middle hearing range (8 and 11.3 kHz, $P = 0.05$, Student's *t*-test), whereas thresholds for other frequencies were similar to those of control animals (Fig. 6B). The amplitude of the DPOAE at 50 dB SPL f2 stimulation level was also slightly, but significantly reduced for *Cacna1d*$^{cko}$ mice (open bars; $P = 0.012$, one-sided *t*-test) when compared with *Cacna1d*$^{fl/fl}$ (closed bar) (Fig. 6C). These data indicate almost normal function of outer hair cells. Next, ABR waves were analyzed. Wave I reflects the summed activity of the auditory nerve, while later waves arise from synchronous neural activity in the auditory brainstem. Wave II is dominated by the response of globular bushy cells in the cochlear nucleus complex (CNC). Wave III is assumed to originate mainly in the CNC and SOC, and the lateral lemniscus and inferior colliculus

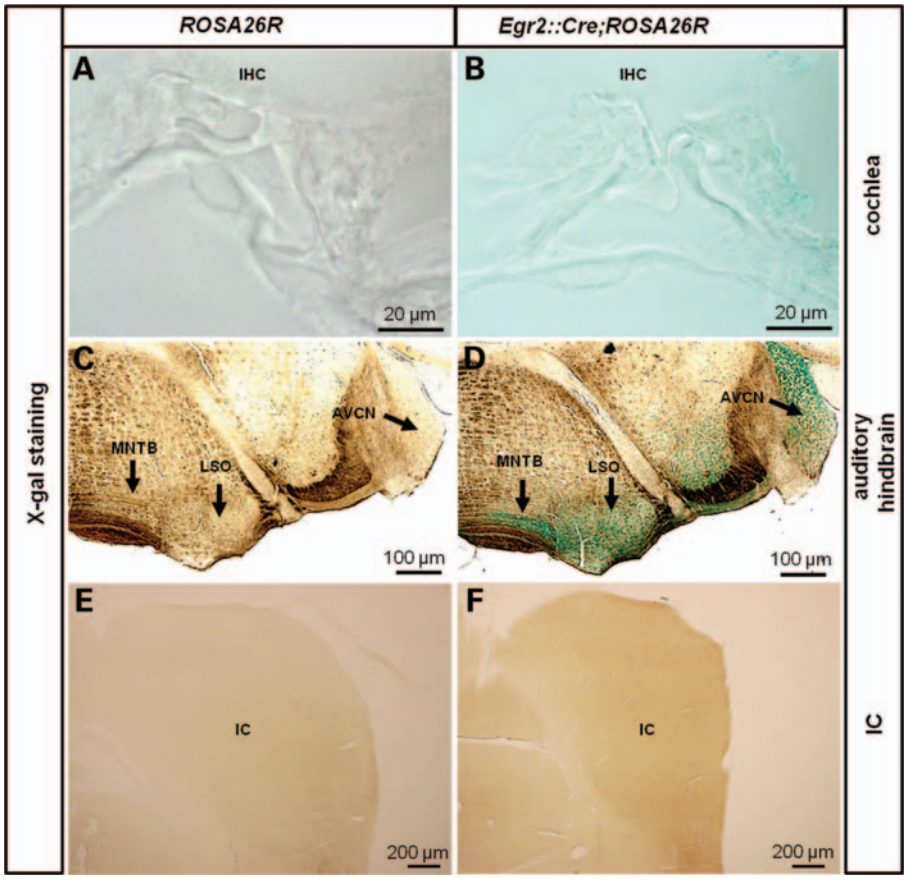


**Figure 3.** Characterization of *Egr2::Cre;ROSA26R* mice. *Egr2::Cre* mice were crossed with *ROSA26R* mice, resulting in expression of β-galactosidase after Cre-mediated recombination, as indicated by the blue staining (**A** and **B**) No X-gal staining was observed in the cochlea of *Egr2::Cre;ROSA26R* mice. Sections are from the midbasal turn. (**C** and **D**) In the CNC, strong X-gal staining was observed in the dorsal cochelar nucleus and the AVCN. In the SOC, strong X-gal staining was present in the LSO and MNTB. (**E** and **F**) In the inferior colliculus, no X-gal staining was observed in the *Egr2::Cre;ROSA26R* mice. Images show representative results from ≥3 independent experiments. AVCN, anteroventral cochlear nucleus; IHC, inner hair cell; IC; inferior colliculus; DCN, dorsal cochlear nucleus; LSO, lateral superior olive; MNTB, medial nucleus of the trapezoid body. In (C)–(F), dorsal is up, lateral is to the right.

contribute to wave-IV (34,35). Deletion of $Ca_v1.3$ resulted in altered ABR waves (Fig. 6D), particularly at high stimulation amplitudes (Fig. 6F). Amplitudes of waves II and III were increased at stimulation levels above 60 dB in *Cacna1d*$^{cko}$ compared with *Cacna1d*$^{fl/fl}$ animals (Fig. 6F). In contrast, wave I amplitudes were slightly decreased between 50 and 75 dB in *Cacna1d*$^{cko}$ (Fig. 6F). This argues against the inner hair cell and spiral ganglion output signal strength as the origin of the higher ABR amplitudes. These data indicate a higher excitability or synchronicity in the CNC and SOC of *Cacna1d*$^{cko}$ mice. Taken together, these physiological data reveal that $Ca_v1.3$ is essential for proper function of the SOC.

### Immunohistochemical analyses of $K_v1$ channels and KCC2

Recently, higher ABR amplitudes were reported in *Kcna1*$^{-/-}$ mice lacking the potassium channel $K_v1.1$ (36). Furthermore, in ubiquitous *Cacna1d*$^{-/-}$ mice, an increase in the firing rate of LSO neurons was linked to reduced expression of $K_v1.2$ (16). To analyze whether the higher ABR amplitudes in waves II and III of *Cacna1d*$^{cko}$ animals are associated with down-regulation of these two channels, immunohistochemical analysis was performed. Both in the LSO and MNTB, we observed strong $K_v1.1$ immunoreactivity in *Cacna1d*$^{cko}$ animals, which was indistinguishable from control animals (Fig. 7A–D). In contrast, immunohistochemistry for $K_v1.2$ revealed a decreased expression in the LSO and MNTB of *Cacna1d*$^{cko}$ animals (Fig. 7E–H). Especially, the intense punctuate staining observed in the processes of control animals was diminished in *Cacna1d*$^{cko}$ animals (Fig. 7E–H, high magnification inserts).

Impaired inhibition, which plays an important role in the auditory brainstem (37), might also contribute to the observed increase in ABR amplitudes. The action of GABA and glycine, the two major inhibitory neurotransmitters in the brain, is determined by the activity of the $K^+$-$Cl^-$ cotransporter KCC2 (38–40). Of note, LTCCs were shown to influence KCC2 expression (41,42). We therefore performed immunohistochemistry for KCC2. Immunolabeling was strong throughout the SOC, including the LSO and MNTB, and no difference in labeling intensity or pattern was visible between control and *Cacna1d*$^{cko}$ animals (Fig. 8A–D). These data demonstrate that the loss of $Ca_v1.3$ affects $K_v1.2$ but not $K_v1.1$ and KCC2 expression. The diminished $K_v1.2$

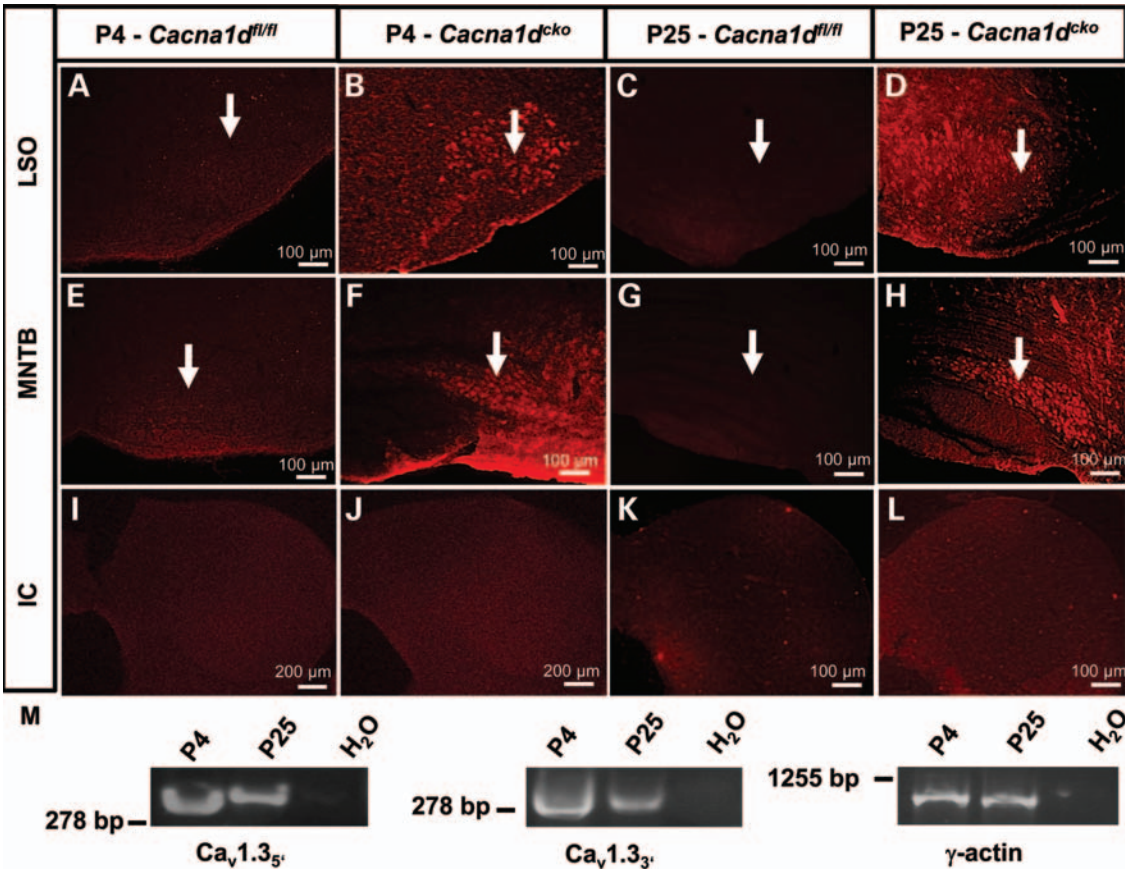


**Figure 4.** Deletion of *Cacna1d* in the SOC of *Cacna1d*$^{cko}$ mice. (**A**–**L**) Crossing of *Egr2::Cre* mice with *Cacna1d-eGFP*$^{flex}$ animals resulted in eGFP expression in auditory brainstem structures, as monitored by immunofluoresence detection with an anti-GFP antibody (depicted as red signal). eGFP immunoreactivity was detected in the LSO (B and D) and the MNTB (F and H) at both P4 (B and F) and P25 (D and H). No immunoreactivity was observed in the inferior colliculus of *Cacna1d*$^{cko}$ mice, which lacks Cre activity (J and K). These data demonstrate deletion of $Ca_v1.3$ in auditory hindbrain neurons. Images show representative results from ≥3 independent experiments. (**M**) Developmental RT–PCR analysis of *Cacna1d* expression in the SOC of P4 and P25 wild-type animals. The presence of *Cacna1d* was investigated using two different primer pairs, which amplify the 5′ part ($Ca_v1.3_{5'}$) and a part towards the 3′ end ($Ca_v1.3_{3'}$) of the open reading frame of *Cacna1d.* At both stages, *Cacna1d* is expressed. Analysis of γ-actin shows a uniform expression across the cDNA pools, indicating equal amounts of cDNA in each RT–PCR reaction. RT–PCRs were performed in duplicate from two biological replica. IC, inferior colliculus; LSO, lateral superior olive; MNTB, medial nucleus of the trapezoid body. In A–L, dorsal is up, lateral is to the right.

expression might contribute to the increased ABR amplitudes of waves II and III in *Cacna1d*$^{cko}$ animals.

### Immunohistochemical analyses of the olivocochlear bundle

In contrast to the increased amplitudes of waves II and III, wave I amplitudes were slightly decreased between 50 and 75 dB despite normal ABR thresholds. One explanation is altered function of the olivocochlear neurons, an efferent feedback system, which regulates cochlear activity (43). Importantly, the somata of olivocochlear neurons reside within two groups of the SOC, the LSO and the ventral nucleus of the trapezoid body (VNTB) (44). To investigate whether these neurons were affected in *Cacna1d*$^{cko}$ mice, we performed immunohistochemistry against ChAT, a marker of these neurons in rodents (44). ChAT-positive neurons were found in the LSO and VNTB and the pattern was indistinguishable between control animals and *Cacna1d*$^{cko}$ mice (Fig. 8E and F). These data suggest that the olivocochlear system is not affected in *Cacna1d*$^{cko}$ mice. However, our data do not exclude that molecular changes within these neurons cause altered feedback to the cochlea.

## DISCUSSION

Here, we show that targeted ablation of $Ca_v1.3$ in the SOC results in abnormalities on the anatomical, molecular and physiological levels. These changes are not reflecting a secondary effect due to the loss of cochlea-driven activity, as ABR thresholds revealed normal function of inner hair cells. The identified abnormalities in the central auditory system therefore reveal a critical role of $Ca_v1.3$ in the auditory system beyond the cochlea. Next to governing neurotransmission from the inner hair cells to the auditory nerve, the protein directly sculptures development and function of central auditory neurons. A dual role in the auditory system was previously established for the transcription factor Gata3, as its loss results in degeneration of hair cells in the cochlea (45) and

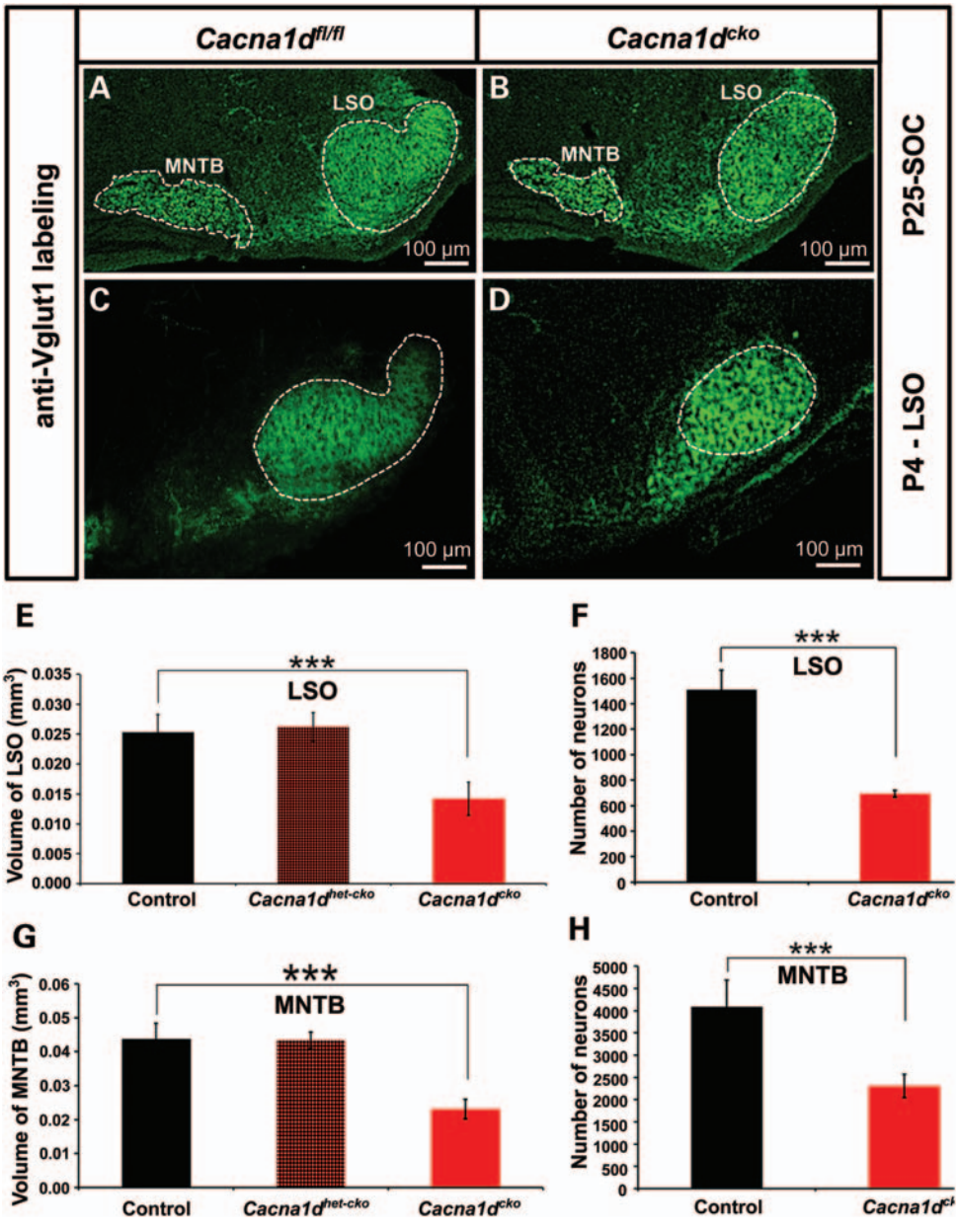


**Figure 5.** Malformed SOC in *Cacna1d*$^{cko}$ mice. (**A** and **B**) Vglut1 immunoreactivity in coronal brainstem sections of P25 control (A) and *Cacna1d*$^{cko}$ mice (B), demonstrating a malformed SOC. (**C** and **D**) The malformed LSO was observed already at P4 in *Cacna1d*$^{cko}$ mice. (**E** and **H**) The volumes and cell numbers of the LSO and MNTB were determined at P25 from Nissl-stained serial sections (six SOCs and three animals per genotype). Significant decrease in the volume and cell number was observed in the LSO (E and **F**) and MNTB (**G** and H) of *Cacna1c*$^{cko}$. LSO, lateral superior olive; MNTB, medial nucleus of the trapezoid body. Dorsal is up, lateral is to the right. $^{***}P < 0.001$; Student's *t*-test.

abnormal projection of olivocochlear neurons in the SOC (9). In the course of our study, such a dual role in the auditory system has been revealed for two more genes. The proneural basic helix-loop-helix transcription factor Atoh1 is essential for hair cell development (46) and proper maturation and function of the auditory brainstem (29). Finally, *Slc17a8,* encoding Vglut3, is required for glutamate release from hair cells (47,48) and circuit refinement of auditory brainstem projections (8). These data bear important clinical implications, as mutations in *Cacna1d* (12), *Gata3* (49,50) or *Slc17a8* (48) have been associated with human hearing loss. In addition to peripheral deafness, affected patients will suffer from gene-specific deficits in the central auditory system. It will therefore be important to decipher the retrocochlear deficits after functional loss of deafness genes in more detail in order to better tailor hearing devices. In certain cases, it might turn out to be more appropriate to use auditory brainstem implants, as already used in patients with neurofibromatosis type 2 (51). The retrocochlear function of at least three peripheral deafness genes also makes a good case for routine functional analyses of deafness genes in the central auditory system.

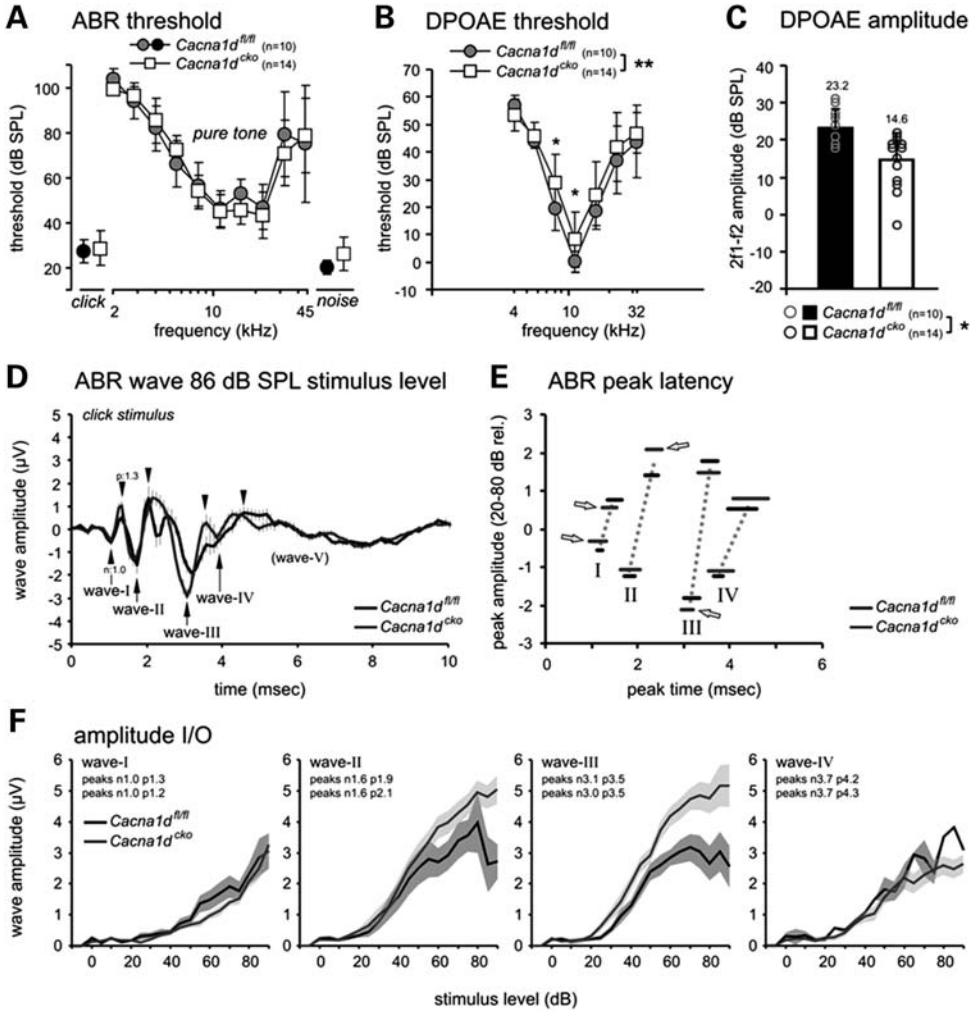


**Figure 6.** Altered ABR in *Cacna1d*$^{cko}$ mice. (**A**) ABR thresholds for pure tone stimuli were invariant between *Cacna1d*$^{fl/fl}$ (control; closed circles) and *Cacna1d*$^{cko}$ mice (open squares; $P > 0.05$, two-way ANOVA). Mean values ± SE are shown. No difference was observed for ABR thresholds in response to click stimuli (lower left corner in the panel) or noise burst stimuli (lower right corner; $P > 0.05$, one-sided *t*-test). (**B**) Thresholds of the 2f1−f2 DPOAE revealed a slight increase in the threshold for 8 kHz and 11.3 kHz in *Cacna1d*$^{cko}$ mice. Statistical significance is indicated for two-way ANOVA analysis comparing the genotype (**) and *post hoc* one-sided *t*-test comparing pairs of thresholds at single frequencies with (*) indicating $P < 0.05$. (**C**) Amplitude of the DPOAE at 50 dB SPL f2 stimulation level (mean values ± SD) was slightly but significantly reduced for *Cacna1d*$^{cko}$ mice (open bars; $P = 0.012$, one-sided *t*-test) when compared with *Cacna1d*$^{fl/fl}$ (closed bar). Individual ear emission signals are shown as circles within each bar. (**D**) Click-evoked ABR waves (mean values ± SE) from *Cacna1d*$^{fl/fl}$ (black) and *Cacna1d*$^{cko}$ (grays) mice for an 86 dB SPL stimulus were overlaid for comparison. ABR wave amplitudes differed between genotypes, and differences were most pronounced at latencies between waves II and IV. The peaks corresponding to ABR wave-I to wave-IV are indicated by the arrows (negative peaks) and arrow heads (positive peaks). Waves are defined by the latency of their leading negative (n) and following positive (p) peak, as illustrated for wave-I. (**E**) Altogether, no difference in peak latencies between *Cacna1d*$^{fl/fl}$ (black) and *Cacna1d*$^{cko}$ (gray), but changes of average peak amplitude for waves I, II and III (arrows, arithmetic mean of ABR peak amplitude for stimuli between 20 and 80 dB). (**F**) Ablation of *Cacna1d* resulted in reduced peak amplitudes in wave I between stimulation levels of 50−70 dB, whereas peak amplitudes increased for waves II and III >60 dB. Average I/O functions from control mice are shown as black lines and from *Cacna1d*$^{cko}$ mice as gray lines (± SE). Data were obtained from 10 to 14 ears per genotype.

Another benefit from a detailed characterization of retrocochlear functions of deafness genes such as $Ca_v1.3$ will be a better insight into the underlying mechanisms and functional consequences of CAPD. These disorders are characterized by impaired sound processing in the central auditory system, which results in the absence of considerable peripheral hearing loss in perceptual dysfunction (52,53). The etiology of CAPD is poorly understood. About 2−3% of children and 10−20% of the elderly are affected. The high prevalence and a 2-to-1 ratio between boys and girls point to a genetic component, and genes important for auditory brainstem function represent attractive candidates. So far, the lack of appropriate clinically exploitable methods for differential diagnosis of the causes have impeded progress in dissection the underlying disease mechanisms by human genetic approaches. Mouse models, such as *Cacna1d*$^{cko}$ mice, therefore represent important tools to explore the pathophysiological processes and functional consequences in CAPD patients.

The mechanisms of action of $Ca_v1.3$ in the central auditory system remain unknown. Nevertheless, its neuronal function

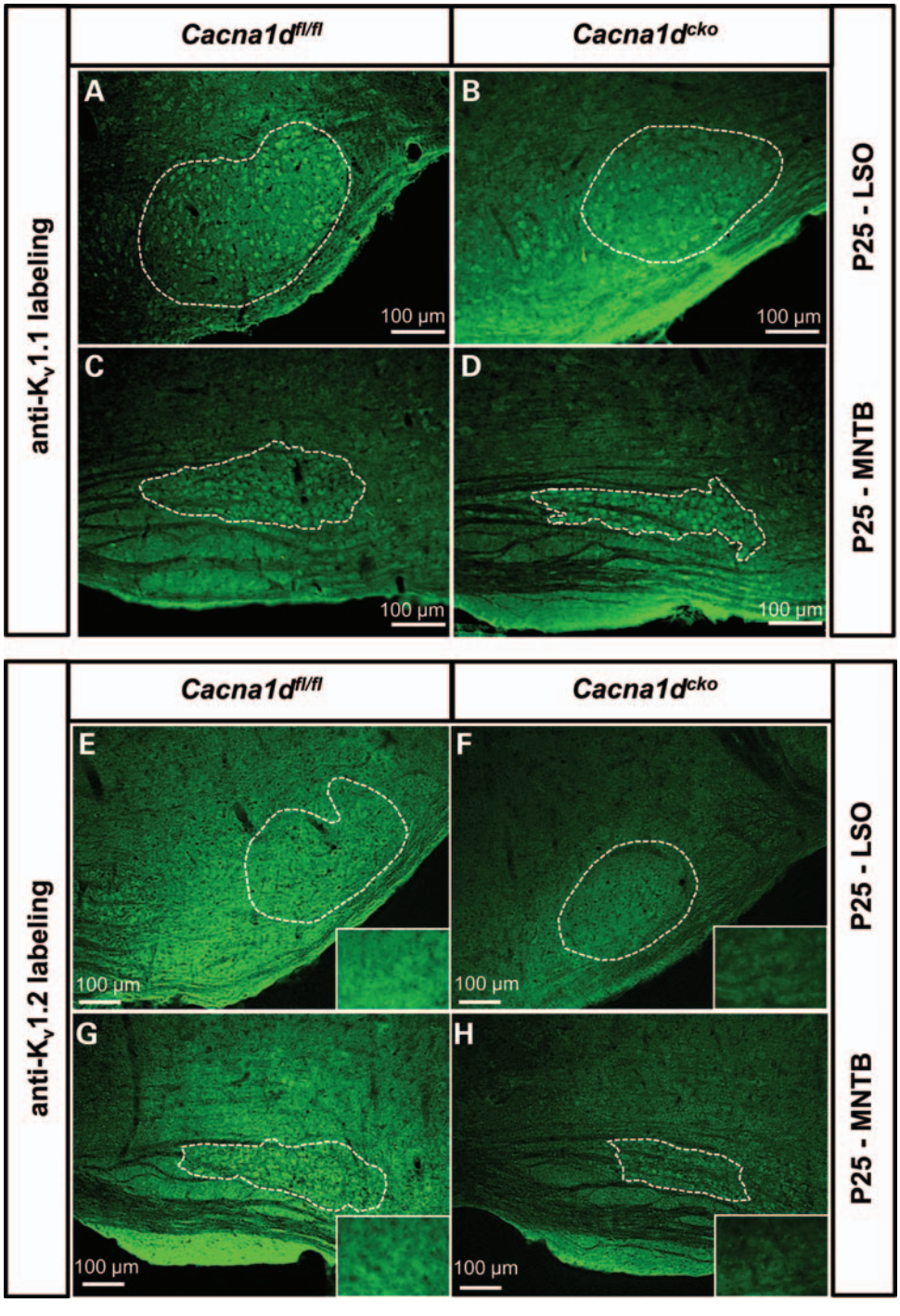


**Figure 7.** Immunohistochemistry of $K_v1$ channels in the SOC of WT and *Cacna1d*$^{cko}$ mice. (**A**–**D**) Strong $K_v1.1$ immunoreactivity was observed in the LSO (A and B) and MNTB (C and D) of WT (A and C) and *Cacna1d*$^{cko}$ (B and D) neurons. (**E**–**H**) Compared with WT mice (E and G), $K_v1.2$ immunoreactivity was reduced in the LSO (F) and the MNTB (H) of *Cacna1d*$^{cko}$ mice. Inserts show high magnifications. Images show representative results from ≥3 independent experiments. LSO, lateral superior olive; MNTB, medial nucleus of the trapezoid body. Dorsal is up, lateral is to the right.

differs from that in sensory hair cells, as the ABR recordings demonstrate neurotransmission in the central auditory pathway of *Cacna1d*$^{cko}$ mice. In neurons, L-type $Ca^{2+}$ channels most often represent an important postsynaptic entry point for signaling cascades involved in excitation–transcription coupling (54–56). In the visual system, for instance, targeted ablation of the calcium channel β3-subunit disrupts axonal refinement (57). Our data demonstrate disturbed SOC architecture already at P4, only few days after the establishment of afferent input. Major SOC nuclei, such as the MNTB, complete their

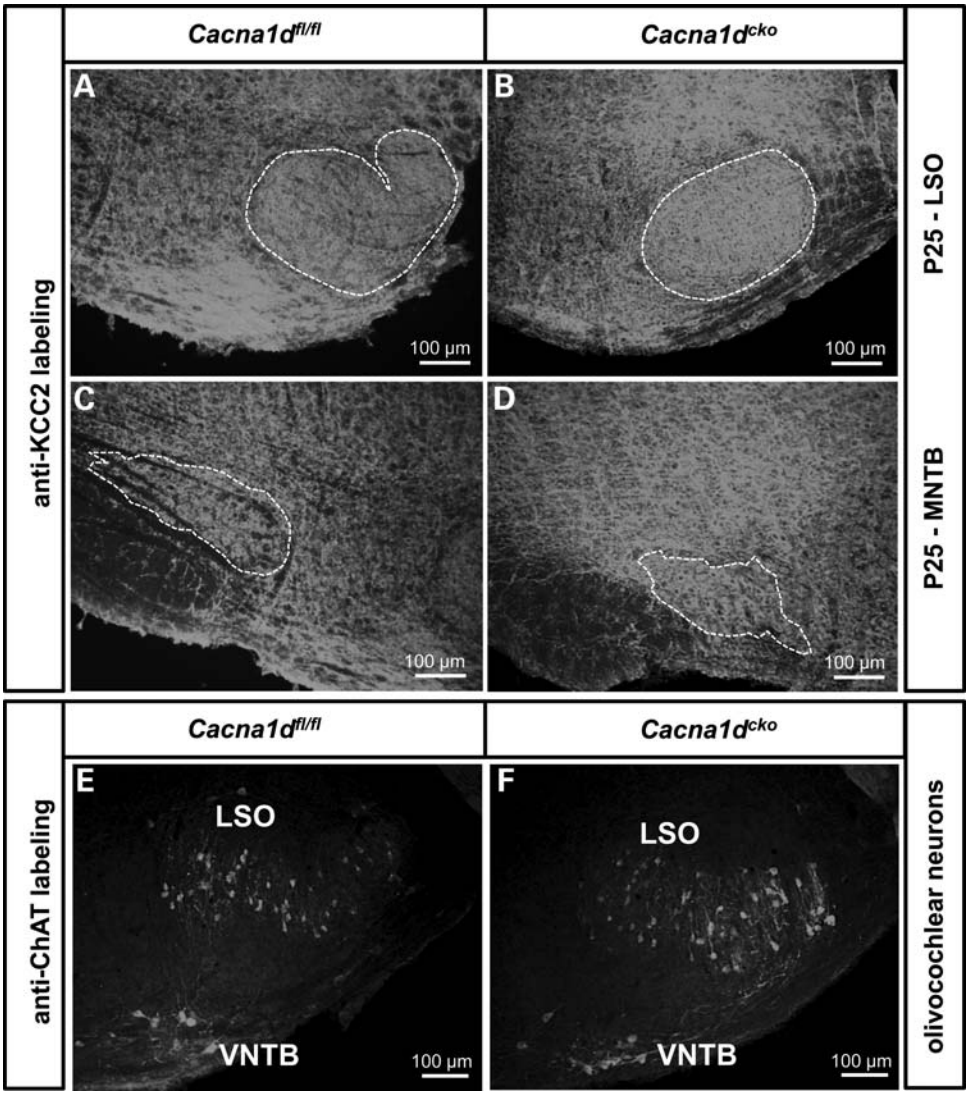


**Figure 8.** Immunohistochemistry against KCC2 and ChAT in the SOC of WT and *Cacna1d*$^{cko}$ mice. (**A**–**D**) Strong KCC2 immunoreactivity was observed in the LSO (A and B), and MNTB (C and D) of WT (A and C) and *Cacna1d*$^{cko}$ (B and D) neurons. (**E** and **F**) Strong ChAT immunoreactivity was observed in the LSO and VNTB of WT (E) and *Cacna1d*$^{cko}$ (F) neurons. These data indicate that KCC2 expression and the olivocochlear bundle are not affected in *Cacna1d*$^{cko}$ animals. Images show representative results from $\geq$2 independent experiments. LSO, lateral superior olive; VNTB, ventral nucleus of the trapezoid body. Dorsal is up, lateral is to the right.

migration approximately 2 days prior to birth (P0 $\approx$ E19) (58,59). At the same day, SOC neurons become functionally innervated by neurons of the anteroventral cochlear nucleus and show elevated $Ca^{2+}$ levels upon presynaptic stimulation (58–60). A crucial role of $Ca_v1.3$ in perinatal excitation–transcription coupling is in agreement with our eGFP expression data in the *Cacna1d*$^{cko}$ mouse and RT–PCR analyses, which demonstrated abundant expression of *Cacna1d* in the SOC from P4 onwards. Furthermore, electrophysiological analyses in transgenic animals revealed functional $Ca_v1.3$ in the SOC of P4- and P12-old animals (17). Support for the importance of signaling cascades between P0 and P4 comes from a previous analysis in mice with ablation of *Atoh1*. In these animals, ~50% of MNTB neurons underwent apoptotic cell death between P0 and P3. It was suggested that this loss reflects a lack of neurotrophic support due to the almost complete absence of their afferent projection neurons (29). Indeed, several analyses demonstrated a tight link between LTCCs and neurotrophic factors. LTCC-mediated $Ca^{2+}$ influx promotes release of brain-derived neurotrophic factor (BDNF) (61) and transcription of the *BDNF* gene in cortical neurons (62) or retinal Müller cells (63). It is therefore interesting to analyze whether $Ca_v1.3$ regulates BDNF levels in the auditory brainstem or whether both act as independent survival promoting factors, as suggested for chicken nodose ganglion neurons (64).

In *Cacna1d*$^{cko}$ mice, neurotransmission from the inner ear to the auditory nerve is preserved. This enabled us to interrogate function of the central auditory brainstem by ABR measurements, which reflect the activity of the auditory brainstem. We observed increased amplitudes of waves II and III in

*Cacna1d*$^{cko}$ animals, which suggest a higher excitation in auditory brainstem nuclei. One explanation is reduced expression of $K_v1$ channels, which are important for rapid repolarization. In constitutive *Cacna1d*$^{-/-}$ mice, pharmacological blocking of $K_v1$ channels by α-dendrotoxin converted LSO neurons with a single firing pattern into neurons with a multiple firing pattern upon current injections (16). Furthermore, loss of this channel reduces inhibitory drive from MNTB neurons into the LSO (65). The reduced expression of $K_v1.2$ in *Cacna1d*$^{cko}$ animals might therefore partially account for the increased ABR amplitudes in waves II and III. However, other proteins might also be affected. For instance, LTCCs mediate activity-dependent up-regulation of $K_v3.1$ in the inferior colliculus, another auditory brainstem structure (66). Detailed expression analyses have therefore to be performed to fully understand the molecular changes giving raise to altered ABRs.

In contrast to waves II and III, we observed between 50 and 70 dB a decrease in the amplitude of wave I, which reflects activity of the auditory nerve. In addition, the DPOAE amplitude was slightly reduced in *Cacna1d*$^{cko}$ mice. Since auditory thresholds are not affected in *Cacna1d*$^{cko}$ mice, we investigated olivocochlear neurons. This efferent feedback system adjusts the sensitivity of the cochlea and influences both the activity of the auditory nerve and DPOAE amplitudes (43,67,68). However, ChAT staining did not reveal any difference on the cellular level between controls and *Cacna1d*$^{cko}$ mice. This finding contrasts observations in mice with targeted ablation of Atoh1, where the loss of SOC neurons resulted in more densely packed and more ventrally located somata of the olivocochlear neurons (29). This difference might be in part due to the apparently stronger reduction in SOC nuclei after targeted ablation of Atoh1 compared with $Ca_v1.3$.

In summary, our analyses identified a crucial role of $Ca_v1.3$ for the development of central auditory centers, and *Cacna1d*$^{cko}$ mice will provide a valuable mouse model to study CAPD. Furthermore, the newly generated *Cacna1d-eGFP*$^{flex}$ paves the way for spatial and temporal control of $Ca_v1.3$ loss, which will result in better tailored mouse models to study the physiological and pathophysiological roles of the channel.

## MATERIALS AND METHODS

### Animals

The Cre lines *Egr2::Cre* (28) and *EIIa::Cre* (19), the Cre-reporter line *ROSA26R* (69) and the Flpe-deleter mouse (70) were described previously. All protocols were in accordance with the German Animal Protection law and approved by the local animal care and use committee (LAVES, Oldenburg, Karlsruhe). Protocols also followed the NIH guide for the care and use of laboratory animals.

### Generation of the *Cacna1d-eGFP*$^{flex}$ mouse line

To generate mice with a conditional *Cacna1d-eGFP*$^{flex}$ allele, exon 2 of *Cacna1d* was targeted, as its ubiquitous deletion resulted in a complete silencing of the gene (11). The exon trapping cassette consisted of the promoterless reporter gene *eGFP* with an upstream general adenovirus splice acceptor and a downstream transcriptional termination sequence (polyadenylation sequence) (71). As a template for the *Cacna1d* locus, the cosmid J14279Q4 from a Lawrist7 genomic library of the 129 mouse strain was obtained from the RZPD (Berlin, Germany). The cassette was flanked by one pair of wild-type *loxP* sites and one pair of mutant *L3* sites, with alternate organization and head-to-head orientation within each pair (Fig. 1A). This organization results in an inversion of the floxed cassette upon *Cre* expression (18). For positive selection in embryonic stem (ES) cells, the construct contained an FRT-flanked neomycin resistance gene (*neo*). The cassette was flanked on the 5′ end by a 2.6 kb homology arm encompassing exon 1a and at the 3′ end by a 5.6 kb homology arm containing exon 3. A thymidine kinase from Herpes simplex virus was introduced downstream to the 3′ homology arm as a negative selection marker (Fig. 2A). Recombineering techniques based on phage recombination were used to assemble the construct (72). To analyze functionality of the resulting construct in HeLa cells, the Caggs promoter [chicken beta-actin promoter with CMV enhancer (73)] was cloned into the 5′ homology arm 2 kb upstream of *eGFP*. The final targeting construct (without the Caggs promotor) was electroporated into R1 ES cells (74), which are derived from agouti-colored 129/SvJ mice. Positive ES cells were injected into blastocysts derived from the mouse strain C57Bl6n. To remove *neo*, heterozygous *Cacna1d-eGFP*$^{flex/+}$ mice were crossed with the Flpe-deleter mouse strain, which expresses the Flpe recombinase under the promoter of the human ACTB gene (Tg(ACTFLPe)9205Dym/J). This promoter is active in almost all tissues, including germ cells (70). The resulting germline knock-in of eGFP into the *Cacna1d* gene was maintained and analyzed as a heterozygote in the absence of the *Cre* allele. The *Egr2::Cre* allele was genotyped with primers 5′-CACTACACCAGCAACTCCTGGCTCC-3′ and 5′-ATGCTCAGAAAACGCCTGGCGATCC-3′. The *Cacna1d-GFP*$^{flex/+}$ allele was identified with primers 5′-GGAGTTGTGT ATATCTGTTAAGCCATG-3′ and 5′-CTCGTTCATATTCTA ACTCCCTA-3′ (product sizes: 2448 bp from the recombined *Cacna1d-GFP*$^{flex/+}$ locus and 1000 bp from the wild-type *Cacna1d* locus).

### RT–PCR analysis

For RT–PCR analyses of the mouse SOC, the brainstem was dissected from animals aged P4 or P25 and 200-μm-thick coronal sections were cut with a vibratome (Leica VT 100 S, Leica, Nussloch, Germany). Subsequently, the SOC was dissected manually. At P4, SOCs were bilaterally collected from one slice and at P25 from three slices. For RNA isolation, SOCs from five P4 animal or two P25 animals were pooled for each biological replica. Total RNA was isolated by the guanidine thiocyanate method (75). After reverse transcription, PCR was performed with primer pairs $Cacna1d_{5'}$-for 5′-TGCAACATCAACGGCAGCAC-3′ and $Cacna1d_{5'}$-rev 5′-CTAATGCAGGCTCTTCGGATG-3′ (334 bp product) to amplify the 5′ of the open reading frame of *Cacna1d*, $Cacna1d_{3'}$-for 5′-ACATTCTGAACATGGTCTTCACAG-3′ and $Cacna1d_{3'}$-rev 5′-AGGACTTGATGAAGGTCCACAG-3′ (283 bp product) to amplify a part towards the 3′ of

*Cacna1d* (76), and γ-actin-for 5′-ACAATGGCTCCGGCA TGTGC-3′ and γ-actin-rev 5′-CCACATCTGCTGGAA GGTGG-3′ (1029 bp product) at an annealing temperature of 56°C for 30 cycles. PCR products were analyzed in a 2% agarose gel.

### DAB staining, immunofluorescence and X-gal staining

For DAB staining, tissue sections were permeabilized in 1% $H_2O_2$ in phosphate-buffered saline (PBS) (150 mM NaCl, 10 mM Na-phosphate, pH 7.4) for 10 min at room temperature and washed with PBS three times for 10 min. To block unspecific binding sites, sections were incubated in 2% normal goat serum in 1% BSA/0.3% Triton X-100/PBS for 1 h at room temperature. The primary antibody anti-GFP (Molecular Probes Invitrogen, Karlsruhe, Germany) was diluted 1:5000 in blocking solution and slices were incubated at 4°C over night. After two washes in 0.3% BSA/0.1% Triton X-100/PBS, slices were incubated for 1 h at room temperature with the biotinylated secondary anti-rabbit IgG antibody (Vector Laboratories, Lörrach, Germany), diluted 1:600 in 0.3% BSA/0.1% Triton X-100/PBS. Thereafter, slices were washed twice in the same buffer without antibody. To enhance staining, sections were incubated with an avidin-biotin complex for 1 h followed by one washing step in 0.3% BSA/0.1% Triton X-100/PBS and two washing steps with PBS. Sections were then incubated in DAB solution (0.4 mg/ml) in 20 mM Tris–HCl with 0.012% $H_2O_2$ until staining was observed. The reaction was stopped by washing three times with PBS. Stained slices were mounted on glass slides and cover slipped with Eukitt (Sigma Aldrich, Taufkirchen, Germany). Slices were imaged with a stereoscope (Stemi 2000-C, Zeiss, Oberkochen, Germany).

For immunohistochemistry, a rabbit anti-GFP antibody was obtained from Invitrogen, a goat anti-ChAT from Millipore (Schwalbach, Germany), the mouse anti-$K_v$1.1 and anti-$K_v$1.2 from Neuromabs (Davis, USA), anti-KCC2 was reported previously (77) and rabbit anti-Vglut1 antibody was a generous gift from Dr S. El Mestikawy (Creteil, Cedex, France). During immunohistochemistry against eGFP, the experimenter was blind to the genotype for two experiments for each stage and assigned eGFP expression correctly to the genotype. All comparisons between wild-type and knockout animals were done on slices processed strictly in parallel on the same day. Antibodies were diluted 1:2000 (anti-GFP), 1:200 (anti-ChAT), 1:50 (anti-$K_v$1.1 or anti-$K_v$1.2), 1:500 (anti-KCC2) and 1:1500 (anti-Vglut1) with carrier solution containing 1% bovine serum albumin, 1% goat serum and 0.3% Triton X-100 in PBS. Sections were incubated overnight with agitation at 7°C. They were then rinsed three times for 10 min in PBS, transferred again to carrier solution and incubated with secondary antibodies coupled to Alexa Fluor Dyes (diluted 1:1000, Invitrogen) for 1–2 h. After several washes in PBS, slices were mounted and images were taken with a BZ 8100 E fluorescence microscope (Keyence, Neu-Isenburg, Germany). When comparing immunoreactivity in wild-type and knockout mice, images were taken under identical conditions for a given antibody. Image data were processed using Adobe Photoshop 7.0 software (Adobe Systems).

Nissl staining was performed on 30-μm thick sections. The volume of auditory nuclei was calculated by multiplying the outlined area with the thickness of each section (16). Three animals were analyzed for each genotype. For X-gal staining of brain sections, mice were perfused transcardially with a buffer containing 1× PBS, 1% formaldehyde, 0.2% glutaraldehyde, 0.2% NP-40 and 0.1% cholic acid. X-gal staining was performed in the following staining solution: 1× PBS, 2 mM $MgCl_2$, 5 mM $K_3Fe(CN)_6$, 5 mM $K_4Fe(CN)_6$, 1 mg/ml X-gal, 0.2% NP-40 and 0.1% cholic acid. Cochleae were decalcificied in Rapid Bone Decalcifier (Apex Engineering Producers Corporation, IL, USA) and cryosectioned at 10 μm. Slices were postfixed in 4% PFA and 2.5% glutaraldehyde and stained in X-gal solution for 24–48 h at 37°C prior to analyses using a Keyence BZ 8100 E microscope (brain slices) or an Olympus AX70 microscope (cochlea). Statistical analysis was performed using Student's *t*-test.

### Auditory evoked brainstem responses and otoacoustic emissions

ABR and DPOAEs were recorded in 6–9-week-old mice, anesthetized with a mixture of ketamine hydrochloride (75 mg/kg body weight, Pharmacia, Erlangen, Germany) and xylazine hydrochloride (5 mg/kg body weight, Bayer, Leverkusen, Germany). Electrical brainstem responses to free field click (100 μs), noise burst (1 ms) and pure tone (3 ms, 1 ms ramp) stimuli were recorded with subdermal silver wire electrodes at the ear, the vertex and the back of the animals. After amplification and bandpass filtering (200 Hz–5 kHz), signals were averaged for 64–256 repetitions at each sound pressure presented (usually 0–100 dB SPL in steps of 5 dB). Thresholds were determined by the lowest sound pressure that produced visually distinct evoked potentials from above threshold to near threshold. The cubic 2f1 − f2 DPOAE was measured for f2 = 1.24 × f1 and L2 = L1 − 10 dB. Emission signals were recorded during sound presentation of 260 ms and averaged four times for each sound pressure and frequency presented. First, the 2f1 − f2 distortion product amplitude was measured with L1 = 50 dB SPL and f2 between 4 and 45.2 kHz. Subsequently, the 2f1 − f2 distortion product amplitude was measured for L1 ranging from −10 to 65 dB SPL at frequencies of f2 between 4 and 32 kHz.

Average ABR-wave curves are presented as mean ± SE. Peak amplitudes and latencies were collected, grouped in clusters of similar peak amplitudes and latencies and averaged for ABR-wave input–output analysis. Clusters of peaks were found at average latencies n0.9-p1.2 (wave I), n1.5-p2.2 (wave II), n2.9-p3.5 (wave III) and n3.9-p4.9 (wave-IV) (n = negative peak, p = positive peak, number = peak latency in ms). Differences of the mean were compared for statistical significance by Student's *t*-test, alpha-levels corrected for multiple testing by Bonferroni–Holms, and two-way ANOVA (GraphPad Prism 2.01). Statistical significance was tested at alpha = 0.05, and resulting *P*-values are reported in the text and figures.

## ACKNOWLEDGEMENTS

We wish to thank Anja Feistner, Jasmin Schröder, Martina Reents and Ariana Frömmig for excellent technical assistance.

*Conflict of Interest statement*. None declared.

## FUNDING

This work was supported by the EU grant CAVNET (MRTN-CT-2006-035367 to H.G.N. and D.B.), the DFG grants No. 428/5-1 and No. 428/10-1 to H.G.N., the SPP1608, and the BMBF Bernstein Center for Computational Neuroscience Heidelberg/Mannheim 01GQ1003A (TPA3) to D.B.

## REFERENCES

1. Lopez, A.D., Mathers, D.D., Ezzati, M., Jamison, D.T. and Murray, C.J.L. (2006) *Global Burden of Disease and Risk Factors*. The World Bank and Oxford University Press, New York.
2. Steel, K.P. and Kros, C.J. (2001) A genetic approach to understanding auditory function. *Nat. Genet.*, **27**, 143–149.
3. Toriello, H.V., Reardon, W. and Gorlin, R.J. (2012) *Hereditary Hearing Loss and its Syndromes*. Oxford University Press, New York.
4. Petit, C. and Richardson, G.P. (2009) Linking genes underlying deafness to hair-bundle development and function. *Nat. Neurosci.*, **12**, 703–710.
5. Dror, A.A. and Avraham, K.B. (2010) Hearing impairment: a panoply of genes and functions. *Neuron*, **68**, 293–308.
6. Van, E.E., Van, C.G. and Van, L.L. (2007) The complexity of age-related hearing impairment: contributing environmental and genetic factors. *Audiol. Neurootol.*, **12**, 345–358.
7. Teagle, H.F., Roush, P.A., Woodard, J.S., Hatch, D.R., Zdanski, C.J., Buss, E. and Buchman, C.A. (2010) Cochlear implantation in children with auditory neuropathy spectrum disorder. *Ear Hear.*, **31**, 325–335.
8. Noh, J., Seal, R.P., Garver, J.A., Edwards, R.H. and Kandler, K. (2010) Glutamate co-release at GABA/glycinergic synapses is crucial for the refinement of an inhibitory map. *Nat. Neurosci.*, **13**, 232–238.
9. Karis, A., Pata, I., van Doorninck, J.H., Grosveld, F., De Zeeuw, C.I., de, C.D. and Fritzsch, B. (2001) Transcription factor GATA-3 alters pathway selection of olivocochlear neurons and affects morphogenesis of the ear. *J. Comp. Neurol.*, **429**, 615–630.
10. Catterall, W.A. (2000) Structure and regulation of voltage-gated Ca2+ channels. *Annu. Rev. Cell Dev. Biol.*, **16**, 521–555.
11. Platzer, J., Engel, J., Schrott-Fischer, A., Stephan, K., Bova, S., Chen, H., Zheng, H. and Striessnig, J. (2000) Congenital deafness and sinoatrial node dysfunction in mice lacking class D L-type Ca2+ channels. *Cell*, **102**, 89–97.
12. Baig, S.M., Koschak, A., Lieb, A., Gebhart, M., Dafinger, C., Nurnberg, G., Ali, A., Ahmad, I., Sinnegger-Brauns, M.J. and Brandt, N. *et al.* (2010) Loss of Ca(v)1.3 (CACNA1D) function in a human channelopathy with bradycardia and congenital deafness. *Nat. Neurosci*, **14**, 77–84.
13. Helfert, R.H., Snead, C.R. and Altschuler, R.A. (1991) In Altschuler, R.A. (ed.), *Neurobiology of Hearing: The Central Auditory System*. Raven Press, New York, pp. 1–25.
14. Yin, T.C.T. (2002) Neural mechanisms of encoding binaural localization cues in the auditory brainstem. In Oertel, D., Fay, R.R. and Popper, A.A. (eds), *Springer Handbook of Auditory Research: Integrative Functions in the Mammalian Auditory Pathway*. Springer, New York, pp. 99–159.
15. Erazo-Fischer, E., Striessnig, J. and Taschenberger, H. (2007) The role of physiological afferent nerve activity during in vivo maturation of the calyx of Held synapse. *J. Neurosci.*, **27**, 1725–1737.
16. Hirtz, J.J., Boesen, M., Braun, N., Deitmer, J.W., Kramer, F., Lohr, C., Muller, B., Nothwang, H.G., Striessnig, J., Lohrke, S. and Friauf, E. (2011) Cav1.3 calcium channels are required for normal development of the auditory brainstem. *J. Neurosci.*, **31**, 8280–8294.
17. Jurkovicova-Tarabova, B., Griesemer, D., Pirone, A., Sinnegger-Brauns, M.J., Striessnig, J. and Friauf, E. (2012) Repertoire of high voltage-activated calcium channels in lateral superior olive: functional analysis in wild-type, Cav1.3-/-, and Cav1.2DHP-/- mice. *J. Neurophysiol.*, *PMID: 22539826*. [Epub ahead of print].
18. Schnutgen, F., Doerflinger, N., Calleja, C., Wendling, O., Chambon, P. and Ghyselinck, N.B. (2003) A directional strategy for monitoring Cre-mediated recombination at the cellular level in the mouse. *Nat. Biotechnol.*, **21**, 562–565.
19. Lakso, M., Pichel, J.G., Gorman, J.R., Sauer, B., Okamoto, Y., Lee, E., Alt, F.W. and Westphal, H. (1996) Efficient in vivo manipulation of mouse genomic sequences at the zygote stage. *Proc. Natl Acad. Sci. USA*, **93**, 5860–5865.
20. Williams-Simons, L. and Westphal, H. (1999) EIIaCre— utility of a general deleter strain. *Transgenic Res.*, **8**, 53–54.
21. Hell, J.W., Westenbroek, R.E., Warner, C., Ahlijanian, M.K., Prystay, W., Gilbert, M.M., Snutch, T.P. and Catterall, W.A. (1993) Identification and differential subcellular localization of the neuronal class C and class D L-type calcium channel alpha 1 subunits. *J. Cell Biol.*, **123**, 949–962.
22. Kim, M.J., Chung, Y.H., Joo, K.M., Oh, G.T., Kim, J., Lee, B. and Cha, C.I. (2004) Immunohistochemical study of the distribution of neuronal voltage-gated calcium channels in the nNOS knock-out mouse cerebellum. *Neurosci. Lett.*, **369**, 39–43.
23. Davila, N.G., Blakemore, L.J. and Trombley, P.Q. (2003) Dopamine modulates synaptic transmission between rat olfactory bulb neurons in culture. *J. Neurophysiol.*, **90**, 395–404.
24. Tanaka, O., Sakagami, H. and Kondo, H. (1995) Localization of mRNAs of voltage-dependent Ca(2+)-channels: four subtypes of alpha 1- and beta-subunits in developing and mature rat brain. *Brain Res. Mol. Brain Res.*, **30**, 1–16.
25. Wang, X., McKenzie, J.S. and Kemm, R.E. (1996) Whole cell calcium currents in acutely isolated olfactory bulb output neurons of the rat. *J. Neurophysiol.*, **75**, 1138–1151.
26. Hetzenauer, A., Sinnegger-Brauns, M.J., Striessnig, J. and Singewald, N. (2006) Brain activation pattern induced by stimulation of L-type Ca2+-channels: contribution of Ca(V)1.3 and Ca(V)1.2 isoforms. *Neuroscience*, **139**, 1005–1015.
27. Sukiasyan, N., Hultborn, H. and Zhang, M. (2009) Distribution of calcium channel Ca(V)1.3 immunoreactivity in the rat spinal cord and brain stem. *Neuroscience*, **159**, 217–235.
28. Voiculescu, O., Charnay, P. and Schneider-Maunoury, S. (2000) Expression pattern of a Krox-20/Cre knock-in allele in the developing hindbrain, bones, and peripheral nervous system. *Genesis*, **26**, 123–126.
29. Maricich, S.M., Xia, A., Mathes, E.L., Wang, V.Y., Oghalai, J.S., Fritzsch, B. and Zoghbi, H.Y. (2009) Atoh1-lineal neurons are required for hearing and for the survival of neurons in the spiral ganglion and brainstem accessory auditory nuclei. *J. Neurosci.*, **29**, 11123–11133.
30. Farago, A.F., Awatramani, R.B. and Dymecki, S.M. (2006) Assembly of the brainstem cochlear nuclear complex is revealed by intersectional and subtractive genetic fate maps. *Neuron*, **50**, 205–218.
31. Han, Y., Kaeser, P.S., Sudhof, T.C. and Schneggenburger, R. (2011) RIM determines Ca(2)+ channel density and vesicle docking at the presynaptic active zone. *Neuron*, **69**, 304–316.
32. Hafidi, A. and Dulon, D. (2004) Developmental expression of Ca(v)1.3 (alpha1d) calcium channels in the mouse inner ear. *Brain Res. Dev. Brain Res.*, **150**, 167–175.
33. Blaesse, P., Ehrhardt, S., Friauf, E. and Nothwang, H.G. (2005) Developmental pattern of three vesicular glutamate transporters in the rat superior olivary complex. *Cell Tissue Res.*, **320**, 33–50.
34. Henry, K.R. (1979) Auditory brainstem volume-conducted responses: origins in the laboratory mouse. *J. Am. Aud. Soc.*, **4**, 173–178.
35. Galbraith, G., Waschek, J., Armstrong, B., Edmond, J., Lopez, I., Liu, W. and Kurtz, I. (2006) Murine auditory brainstem evoked response: putative two-channel differentiation of peripheral and central neural pathways. *J. Neurosci. Methods*, **153**, 214–220.
36. Allen, P.D. and Ison, J.R. (2012) Kcna1 gene deletion lowers the behavioral sensitivity of mice to small changes in sound location and increases asynchronous brainstem auditory evoked potentials but does not affect hearing thresholds. *J. Neurosci.*, **32**, 2538–2543.
37. Grothe, B., Pecka, M. and Mcalpine, D. (2010) Mechanisms of sound localization in mammals. *Physiol. Rev.*, **90**, 983–1012.
38. Rivera, C., Voipio, J., Payne, J.A., Ruusuvuori, E., Lahtinen, H., Lamsa, K., Pirvola, U., Saarma, M. and Kaila, K. (1999) The K+/Cl- co-transporter KCC2 renders GABA hyperpolarizing during neuronal maturation. *Nature*, **397**, 251–255.

39. Huebner, C.A., Stein, V., Hermans-Borgmeyer, I., Meyer, T., Ballanyi, K. and Jentsch, T.J. (2001) Disruption of KCC2 reveals an essential role of K-Cl cotransport already in early synaptic inhibition. *Neuron*, **30**, 515–524.
40. Balakrishnan, V., Becker, M., Loehrke, S., Nothwang, H.G., Guresir, E. and Friauf, E. (2003) Expression and function of chloride transporters during development of inhibitory neurotransmission in the auditory brainstem. *J. Neurosci.*, **23**, 4134–4145.
41. Ganguly, K., Schinder, A.F., Wong, S.T. and Poo, M. (2001) GABA itself promotes the developmental switch of neuronal GABAergic responses from excitation to inhibition. *Cell*, **105**, 521–532.
42. Bray, J.G. and Mynlieff, M. (2009) Influx of calcium through L-type calcium channels in early postnatal regulation of chloride transporters in the rat hippocampus. *Dev. Neurobiol.*, **69**, 885–896.
43. Guinan, J.J. Jr (1996) In Dallos, P., Popper, A.N. and Fay, R.R. (eds), *The Cochlea*. Springer-Verlag, New York, pp. 435–502.
44. Simmons, D.D. (2002) Development of the inner ear efferent system across vertebrate species. *J. Neurobiol.*, **53**, 228–250.
45. van der Wees, J., van Looij, M.A., de Ruiter, M.M., Elias, H., van der, B.H., Liem, S.S., Kurek, D., Engel, J.D., Karis, A. and van Zanten, B.G. *et al.* (2004) Hearing loss following Gata3 haploinsufficiency is caused by cochlear disorder. *Neurobiol. Dis.*, **16**, 169–178.
46. Bermingham, N.A., Hassan, B.A., Price, S.D., Vollrath, M.A., Ben Arie, N., Eatock, R.A., Bellen, H.J., Lysakowski, A. and Zoghbi, H.Y. (1999) Math1: an essential gene for the generation of inner ear hair cells. *Science*, **284**, 1837–1841.
47. Seal, R.P., Akil, O., Yi, E., Weber, C.M., Grant, L., Yoo, J., Clause, A., Kandler, K., Noebels, J.L. and Glowatzki, E. *et al.* (2008) Sensorineural deafness and seizures in mice lacking vesicular glutamate transporter 3. *Neuron*, **57**, 263–275.
48. Ruel, J., Emery, S., Nouvian, R., Bersot, T., Amilhon, B., Van Rybroek, J.M., Rebillard, G., Lenoir, M., Eybalin, M. and Delprat, B. *et al.* (2008) Impairment of SLC17A8 encoding vesicular glutamate transporter-3, VGLUT3, underlies nonsyndromic deafness DFNA25 and inner hair cell dysfunction in null mice. *Am. J. Hum. Genet.*, **83**, 278–292.
49. Van, E.H., Groenen, P., Nesbit, M.A., Schuffenhauer, S., Lichtner, P., Vanderlinden, G., Harding, B., Beetz, R., Bilous, R.W. and Holdaway, I. *et al.* (2000) GATA3 haplo-insufficiency causes human HDR syndrome. *Nature*, **406**, 419–422.
50. Ali, A., Christie, P.T., Grigorieva, I.V., Harding, B., Van, E.H., Ahmed, S.F., Bitner-Glindzicz, M., Blind, E., Bloch, C. and Christin, P. *et al.* (2007) Functional characterization of GATA3 mutations causing the hypoparathyroidism-deafness-renal (HDR) dysplasia syndrome: insight into mechanisms of DNA binding by the GATA3 transcription factor. *Hum. Mol. Genet.*, **16**, 265–275.
51. Sanna, M., Di, L.F., Guida, M. and Merkus, P. (2012) Auditory brainstem implants in NF2 patients: results and review of the literature. *Otol. Neurotol.*, **33**, 154–164.
52. Chermak, G.D. and Musiek, F.E. (1997) In Chermak, G.D. and Musiek, F.E. (eds), *Central Auditory Processing Disorders*, Conceptual and Historical Foundations, pp. 1–26.
53. Griffiths, T.D. (2002) Central auditory processing disorders. *Curr. Opin. Neurol.*, **15**, 31–33.
54. Cohen, S. and Greenberg, M.E. (2008) Communication between the synapse and the nucleus in neuronal development, plasticity, and disease. *Annu. Rev. Cell Dev. Biol.*, **24**, 183–209.
55. Lonze, B.E. and Ginty, D.D. (2002) Function and regulation of CREB family transcription factors in the nervous system. *Neuron*, **35**, 605–623.
56. Bito, H., Deisseroth, K. and Tsien, R.W. (1997) Ca2+-dependent regulation in neuronal gene expression. *Curr. Opin. Neurobiol.*, **7**, 419–429.
57. Cork, R.J., Namkung, Y., Shin, H.S. and Mize, R.R. (2001) Development of the visual pathway is disrupted in mice with a targeted disruption of the calcium channel beta(3)-subunit gene. *J. Comp. Neurol.*, **440**, 177–191.
58. Hoffpauir, B.K., Kolson, D.R., Mathers, P.H. and Spirou, G.A. (2010) Maturation of synaptic partners: functional phenotype and synaptic organization tuned in synchrony. *J. Physiol.*, **588**, 4365–4385.
59. Marrs, G.S. and Spirou, G.A. (2012) Embryonic assembly of auditory circuits: spiral ganglion and brainstem. *J. Physiol.*, PMID:22371481 [Epub ahead of print].
60. Hoffpauir, B.K., Marrs, G.S., Mathers, P.H. and Spirou, G.A. (2009) Does the brain connect before the periphery can direct? A comparison of three sensory systems in mice. *Brain Res.*, **1277**, 115–129.
61. Porcher, C., Hatchett, C., Longbottom, R.E., McAinch, K., Sihra, T.S., Moss, S.J., Thomson, A.M. and Jovanovic, J.N. (2011) Positive feedback regulation between gamma-aminobutyric acid type A (GABA(A)) receptor signaling and brain-derived neurotrophic factor (BDNF) release in developing neurons. *J. Biol. Chem.*, **286**, 21667–21677.
62. Zheng, F., Zhou, X., Luo, Y., Xiao, H., Wayman, G. and Wang, H. (2011) Regulation of brain-derived neurotrophic factor exon IV transcription through calcium responsive elements in cortical neurons. *PLoS ONE*, **6**, e28441.
63. Sato, T., Fujikado, T., Lee, T.S. and Tano, Y. (2008) Direct effect of electrical stimulation on induction of brain-derived neurotrophic factor from cultured retinal Muller cells. *Invest. Ophthalmol. Vis. Sci.*, **49**, 4641–4646.
64. Larmet, Y., Dolphin, A.C. and Davies, A.M. (1992) Intracellular calcium regulates the survival of early sensory neurons before they become dependent on neurotrophic factors. *Neuron*, **9**, 563–574.
65. Brew, H.M., Gittelman, J.X., Silverstein, R.S., Hanks, T.D., Demas, V.P., Robinson, L.C., Robbins, C.A., Kee-Johnson, J., Chiu, S.Y., Messing, A. and Tempel, B.L. (2007) Seizures and reduced life span in mice lacking the potassium channel subunit Kv1.2, but hypoexcitability and enlarged Kv1 currents in auditory neurons. *J. Neurophysiol.*, **98**, 1501–1525.
66. Liu, S.Q.J. and Kaczmarek, L.K. (1998) Depolarization selectively increases the expression of the Kv3.1 potassium channel in developing inferior colliculus neurons. *J. Neurosci.*, **18**, 8758–8769.
67. Abdala, C., Mishra, S.K. and Williams, T.L. (2009) Considering distortion product otoacoustic emission fine structure in measurements of the medial olivocochlear reflex. *J. Acoust. Soc. Am.*, **125**, 1584–1594.
68. Deeter, R., Abel, R., Calandruccio, L. and Dhar, S. (2009) Contralateral acoustic stimulation alters the magnitude and phase of distortion product otoacoustic emissions. *J. Acoust. Soc. Am.*, **126**, 2413–2424.
69. Soriano, P. (1999) Generalized lacZ expression with the ROSA26 Cre reporter strain. *Nat. Genet.*, **21**, 70–71.
70. Rodriguez, C.I., Buchholz, F., Galloway, J., Sequerra, R., Kasper, J., Ayala, R., Stewart, A.F. and Dymecki, S.M. (2000) High-efficiency deleter mice show that FLPe is an alternative to Cre-loxP. *Nat. Genet.*, **25**, 139–140.
71. Schnutgen, F., De Zolt, S., Van Sloun, P., Hollatz, M., Floss, T., Hansen, J., Altschmied, J., Seisenberger, C., Ghyselinck, N.B., Ruiz, P. *et al.* (2005) Genomewide production of multipurpose alleles for the functional analysis of the mouse genome. *Proc. Natl Acad. Sci. USA*, **102**, 7221–7226.
72. Liu, P., Jenkins, N.A. and Copeland, N.G. (2003) A highly efficient recombineering-based method for generating conditional knockout mutations. *Genome Res*, **13**, 476–484.
73. Niwa, H., Yamamura, K. and Miyazaki, J. (1991) Efficient selection for high-expression transfectants with a novel eukaryotic vector. *Gene*, **108**, 193–199.
74. Nagy, A., Rossant, J., Nagy, R., bramow-Newerly, W. and Roder, J.C. (1993) Derivation of completely cell culture-derived mice from early-passage embryonic stem cells. *Proc. Natl Acad. Sci. USA*, **90**, 8424–8428.
75. Chomczynski, P. and Sacchi, N. (1987) Single-step method of RNA isolation by acid guanidinium thiocyanate-phenol-chloroform extraction. *Anal. Biochem.*, **162**, 156–159.
76. Sinnegger-Brauns, M.J., Huber, I.G., Koschak, A., Wild, C., Obermair, G.J., Einzinger, U., Hoda, J.C., Sartori, S.B. and Striessnig, J. (2009) Expression and 1,4-dihydropyridine-binding properties of brain L-type calcium channel isoforms. *Mol. Pharmacol.*, **75**, 407–414.
77. Blaesse, P., Guillemin, I., Schindler, J., Schweizer, M., Delpire, E., Khiroug, L., Friauf, E. and Nothwang, H.G. (2006) Oligomerization of KCC2 correlates with development of inhibitory neurotransmission. *J. Neurosci.*, **26**, 10407–10419.